

## RESEARCH ARTICLE

# Discovery of Potential Anti-COVID-19 (SARS-CoV-2) Compounds using Interaction-Pharmacophore Modeling

Apurba K Bhattacharjee\*

*Biomedical Graduate Research Organization, Department of Microbiology and Immunology*

*School of Medicine, Georgetown University, Washington, United States*

**\*Corresponding author:** Apurba K Bhattacharjee, Biomedical Graduate Research Organization, Department of Microbiology and Immunology, School of Medicine, Georgetown University, Washington, DC 20057 (U.S.A.), Tel: 001-301-438-8196, E-mail: ab3094@georgetown.edu

**Citation:** Apurba K Bhattacharjee (2021) Discovery of Potential Anti-COVID-19 (SARS-CoV-2) Compounds using Interaction-Pharmacophore Modeling. J Med Chem Drug Design 1: 102

## Abstract

In this study, computations were performed on seven drugs used for SARS-CoV-2 (COVID-19) treatments to develop a reliable model to enable search for new potentially less toxic anti-COVID-19 compounds. Stereo-electronic properties and “pharmacophores” were determined and interaction capabilities were compared with an inhibitor bound x-ray crystallographic structure of the main protease 3CL-protease (MPro). Based on similarity of “interaction-pharmacophore profiles”, a literature search was carried out which led to identify eleven new compounds. They include isoquine and several 4-aminoquinolines having the potential for activity against COVID-19. The results are discussed to account for activity of both the used drugs and identified compounds. This rational approach may aid the urgent need for rapid discovery of compounds having the potential for COVID-19 activity.

**Keywords:** SARS-CoV-2 (COVID-19) Drugs, Interaction Pharmacophores, Antimalarial Aminoquinolines, 3CL Protease Crystallographic Structure (MPro).

## Introduction

Novel coronavirus caused by SARS-CoV-2 (COVID-19), first appeared in late 2019 as a mysterious pneumonia like illness in Wuhan, China [1]. The infection had quickly emerged as a pandemic engulfing the entire world. As of 25 April 2021, the virus has already infected more than hundred and forty million people and killed approximately 3.1 million people worldwide [2] and the numbers are rising daily.

Currently, there is no proper drug to treat the infection effectively and stop the spread of COVID-19. With thousands of new cases developing daily and hundreds of fatalities, finding a drug to prevent or treat the infection effectively is the pressing need for the research community. Clinical symptoms of the infection were reported to include fever, cough, shortness of breath, and fatigue while CT scan imaging demonstrated pneumonia in the chest for patients [3].

Developing new therapies and putting them through clinical trials and regulatory processes is a long and expensive process. However, finding drugs that are already FDA- approved could be an effective alternative for the possible early mitigation of the infection. The approach could be potentially more expedient as a new application rather than the lengthy process of discovery of a new drug molecule. This type of drug repurposing strategy (also known as drug repositioning) offers a quick path to a successful and cost effective development of new treatments for sudden emergence of novel diseases. The process for exploring additional value for an existing drug by targeting a disease has significant advantages over new drug discovery [4, 5]. Since steps for chemical synthesis, manufacturing processes, safety profiles, and pharmacokinetic properties in pre-clinical including animal studies along with early clinical studies (phase 1, 2 and possibly 3) are already known, the approach could have a higher probability for success compared to developing an altogether new molecule. Moreover, the process of repurposing of an old FDA-approved drug will not only be less expensive but may rapidly be available [6-8] than the alternative process of new drug discovery. Remdesivir, chloroquine (CQ), and hydroxychloroquine (HCQ) are such repurposed drugs currently being used against COVID-19 despite their certain toxicity issues [1, 3].

In pursuit of these goals, the present study attempts to identify potential anti-COVID-19 compounds having potentially less toxicity through theoretical approaches. Specific goal was to develop an *in silico* “interaction pharmacophore” model from the nine known FDA-approved drugs (Table 1, Chart 1) which are already been used for treatments against SAR-Cov-2 (Covid-19) [9-11] and utilize the model to identify new potential anti-COVID-19 compounds. The theoretical model was developed using density functional and semi-empirical quantum chemical computations and analysis of stereo-electronic properties of the drugs. The model was validated by analyzing the consistency in interactions observed from the x-ray crystallographic structure of COVID-19 main protease (Mpro), the 3CL-protease bound with a ligand [12].

Although all drugs (Table 1, Chart 1) used for developing the model may not have the same mechanism of action of interactions with proteases, the hydrogen bonding ability of the drugs are known to be a common factor in the molecular mechanism of action with the receptor. Since the M-protein is most abundant in viral surfaces and it is believed to be the central organizer for the coronavirus assembly and many HIV-1 protease inhibitors, tipranavir, saquinavir, ritonavir, nelfinavir, lopinavir, indinavir, darunavir, atazanavir, and amprenavir are widely reported to be able to deactivate Mpro [13], we focused on this protein crystal structure for the design of anti-COVID-19 compounds. Furthermore, MPro also became very attractive target due to literature reports of several crystal structure of COVID-19 Mpro in complex with different inhibitor in the protein data bank [13] (<https://pdj.org/featured/covid-19>).

Interestingly, the model developed us led to identify several potential anti-COVID-19 aminoquinoline derivatives from a literature survey. A few of these aminoquinolines are FDA approved drugs for malaria treatments and preventive therapies. One of the main identified compounds, N-tert-butyl isoquine (GSK369796) is not only an effective antimalarial but also known to be a potent anti-dengue and Zika antiviral agent as well as has the ability for inhibiting the hERG potassium ion channel repolarization [14, 15].

## Materials and Methods

### Calculation of Stereo-Electronic Properties

Computational calculations were performed using SPARTAN'18 version v1.4.6 [16] running on a laptop MacBook Pro with macOS Catalina 10.15.6 workstation. Detailed conformational search calculations of all compounds Table 1 (Chart 1 & 2) were performed by multiple rotations of single bonds in the compounds, thereby generating several low-energy conformers with varying population densities. Normally, the conformational energies of conformers statistically significant are between 0.0 and 20.0 kcal/mol are considered for further computations since these conformers are easily surmountable in the highly dynamic target proteins and are thermodynamically stable. Thus, any such conformer is likely to be potently active in binding with the protein. The most abundant and the lowest energy conformers were identified. The geometry of these conformers was optimized, and the electronic properties were calculated on the optimized geometry. Geometry optimization and energy calculations were performed in the gas phase state of compounds using first the semi-empirical PM3 (Parameterized Model number 3) followed by DFT (density functional theory with wb97X-D, 6-31G\* basis sets) methods of quantum chemical theory [16]. The PM3 optimized geometry was further optimized using the DFT methods for obtaining a better accuracy of the model and less expensive approach in terms of computation time than Hartree-Fock (HF) models [17, 18].

Three-dimensional molecular electrostatic potential (MEP) maps for the compounds were generated using SPARTAN graphics [16] on the DFT-optimized geometry. The electrostatic potentials were sampled over the entire accessible surface of a molecule (corresponding roughly to a van der Waals contact surface) and into space extending beyond the molecular surface providing a measure of charge distribution from the point of view of an approaching reagent. The MEP profiles were also generated on the beyond the van der Waals surface in the range from approximately, -80.0 to -20.0 kJ/mol (-20.0 to -5.0 kcal/mol) because these are the profiles recognized by the target molecule at a distance to promote interaction with the target. These color-coded van der Waals isosurfaces (at constant electron density of 0.002 e/au<sup>3</sup>) provide an indication of overall molecular size and of location of negative or positive electrostatic potentials. The most negative electrostatic potential is colored deepest red, and the most positive electrostatic potential is colored deepest blue. These MEP profiles of compounds are known as the “interaction pharmacophores”. In addition, other molecular electronic properties such as the molecular orbital energies, dipole moments, octanol/water partition coefficients (logP), and other structural parameters were calculated on the optimized geometry and profiles for each molecule was developed using the SPARTAN'18 graphics [16].

### Pharmacophore development from Chemical Function Descriptors (CFD's)

CFD's are descriptors assigned to a molecule based on its chemical features to characterize commonality between molecules with different structures. We used Spartan' 18 [16] to develop the models. Spartan18 provides seven different kinds of CFDs: (1) hydrophobic, (2) aromatic, (3) hydrogen-bond donor, (4) hydrogen-bond acceptor, (5) positive ionizable site, and (6) negative ionizable site. The seventh CFD type, excluded volume, derives from knowledge of a molecule incorporated into the host protein. Excluded volumes may be obtained for ligands extracted from PDB files.

CFD's and other functional groups may that depend on the pH. At neutral (or basic) pH this CFD should be designated both as a hydrogen-bond donor and a hydrogen-bond acceptor, whereas at acidic pH it should be designated as a negative ionizable site. Finally, it may be noted that default assignments for hydrogen-bond donors and acceptors depend not only on atomic type (N, O, . . .) and (in the case of hydrogen-bond donors) on the availability of hydrogens, but also on known (or presumed) chemical behavior. For example, since an amide nitrogen would not generally be considered to be a hydrogen-bond acceptor, it will be assigned as a hydrogen-bond donor, if of course, hydrogens are available but the amide oxygen is assigned as a hydrogen-bond acceptor.

Furthermore, the hydrogen-bond acceptor and donor CFD's can be related to electrostatic potentials obtained from the quantum chemical calculations. For example, a negative potential associated with an oxygen center suggests that it might serve as a hydrogen-bond acceptor, while a positive potential associated with a hydrogen suggests its role as a hydrogen-bond donor. While a

chemist would reach the same conclusions simply by looking at the molecule, the calculations should be provide better estimate of the strength of H-bond acceptor or donor sites. Calculated electrostatic potentials may offer significant advantage over CFD's and other qualitative descriptions when there are no heteroatoms and hydrogen bonding is not possible. The  $\pi$  system of benzene and other aromatics provide the most common examples. The same conditions that make the ring susceptible to electrophilic aromatic substitution mean that it repels other electron-rich regions (and attracts electron-poor regions).

### Similarity analysis between molecules from CFDs

Similarity analysis was carried on the basis of CFD's in the molecules. This analysis provides insight between atom centers in different molecules regarding their likely functions as a hydrogen-bond donor or hydrogen-bond acceptor. That is to say, whether an atom center is likely to act on a positive or a negative charge or is hydrophobic. The computer time required for similarity analysis is based on the number of molecules and/or pharmacophores in the query, the number of molecules and/or pharmacophores in the library and the nature of the selected CFD's in the query. For each query/library pair, where the query is represented by  $i$  CFD's of type A,  $j$  CFD's of type B,  $k$  CFD's of type C, etc., the number of different alignment combinations that need to be considered is given by the factorial equation:

$$i!j!k! \dots$$

(Where! is the factorial symbol.) The calculation rapidly becomes unmanageable. For example, if there are 6 CFD's of type A, 3 of type B and 2 of type C, the number of combinations is  $6!3!2!$  or 8640. By limiting the number of CFD's of a given type in the overall representation faster calculations can be achieved [16].

#### 2.4. Structure based pharmacophore development:

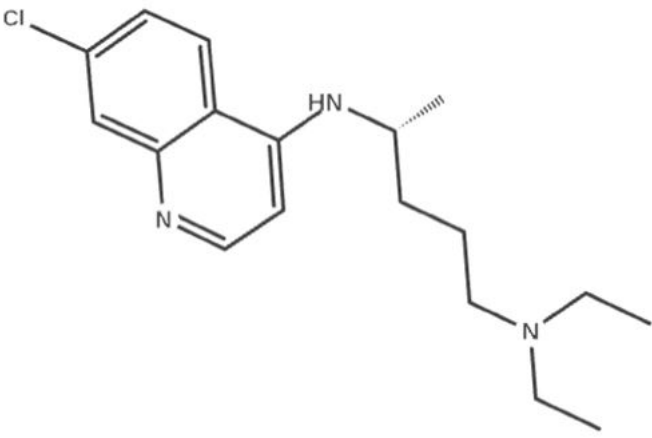
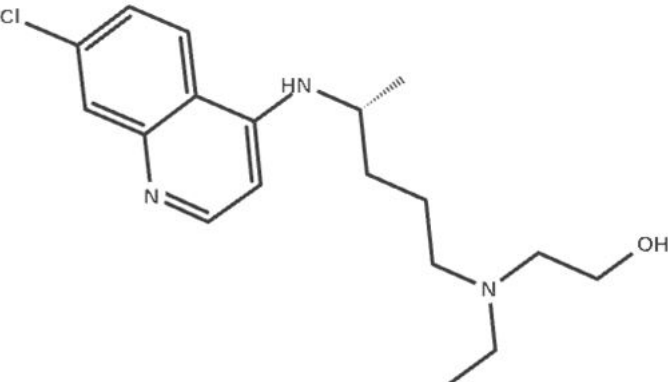
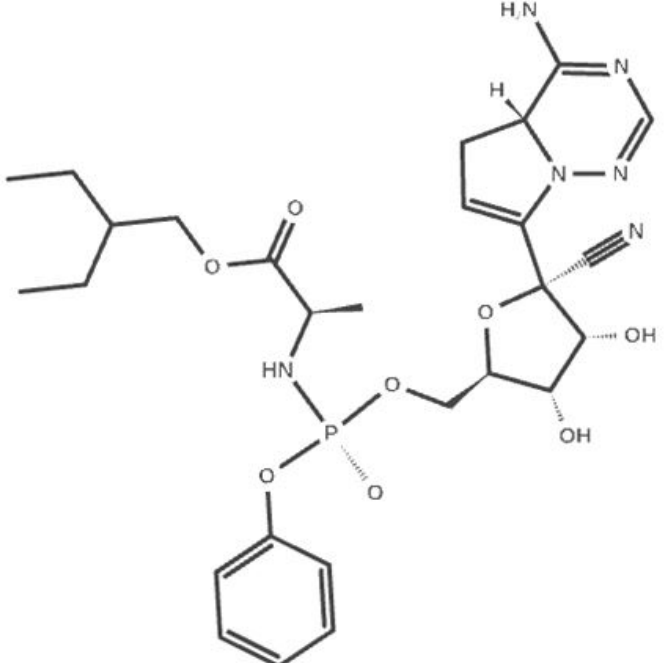
The 3D coordinates of COVID-19 main protease complexed with the inhibitor; X77, was downloaded from the Protein Data Bank. (PDB code: 6W63, 2.10 Å) (<https://www.rcsb.org/>) [12, 13]. Hydrogen atoms were added to the proteins utilizing Spartan'18 templates for protein residues and the water molecules were kept in the protein structure. The protein- inhibitor complex was carefully explored to identify the intermolecular interactions, only those interactions within 3 Å were considered to develop a manual structure-based pharmacophore.

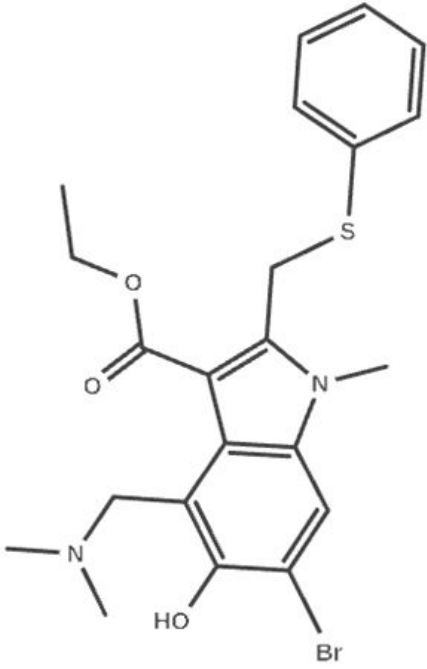
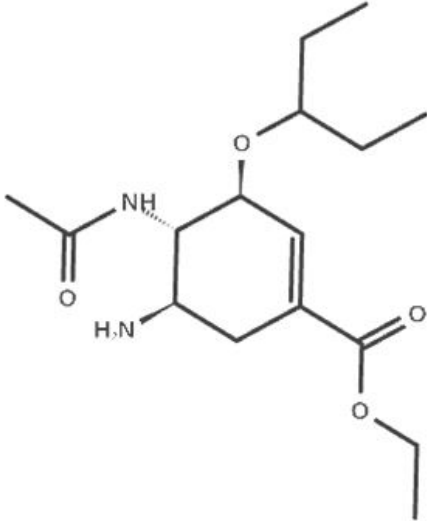
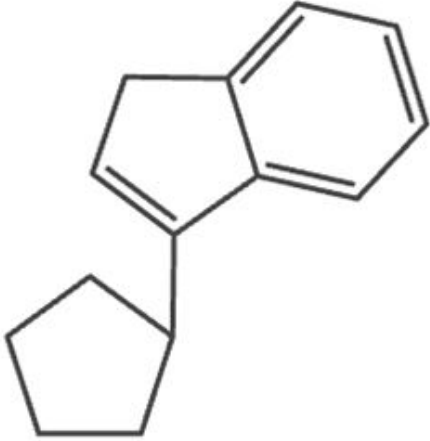
## Results and Discussions

Structure of COVID-19 drugs (Table 1, Chart 1) for which the "interaction pharmacophores" were developed include chloroquine (CQ) and hydroxychloroquine (HCQ), remdesivir, arbidol, oseltamivir, galidesivir, and favipiravir. These compounds were used in different stages for treatments of COVID-19 as mentioned earlier [9-11]. In addition, the (Table 1, Chart 1) shows the structure of an inhibitor (X77- ligand) found in the bound 3CL-protease (Mpro) crystallographic structure [12]. Structures of compounds identified from literature search using the "interaction pharmacophore" model are shown (Table 1, Chart 2).

### Stereoelectronic property computations

Geometry of all compounds was optimized using methods from quantum chemistry. Results of calculated stereoelectronic properties on the optimized geometry of compounds are presented in Table 2 & 3. Analysis of Table 2 & 3 indicates a few general observations. For example, dipole moment most of the compounds is less than 6.0 debye units pointing towards the quinolone ring N atom, Log P is less than 2.0, and a polar surface area (PSA) of less than 50.0 Å<sup>2</sup>. Drug-likeness properties as reported in the set of empirical rules by Lipinsky et al [19(a),(b)], compounds of both Table 1 (Chart 1 & 2) appear to have favorable drug-likeness properties. For example, molecular weight (<500), clogP (<5.00), polar surface area, PSA (<140 Å<sup>2</sup>), number of H-bond acceptors (<10.0), number of H-bond donors (<5.0) are common to all except Compound 3 (Table 1, Chart 1, remdesivir). However, considering the number of rotatable bonds as drug-likeness to be <10, two compounds, Compound 3 (Table 1, Chart 1), (remdesivir) and Compound 9' (Table 1, Chart 2), (cycloquine), do not support the requirements for the empirical rule. None of the compounds is a peptide and all of them contain aromatic rings and less than two carboxylic acid moieties. Thus, considering the drug likeness properties, it would be reasonable to comment that compounds of both Table 1 (Chart 1&2) should have favorable solubility, permeability, bioavailability, volume of distribution, plasma protein binding, CNS penetration, and blood-brain barrier properties except the two compounds mentioned above [20].

1	Chloroquine	 <p>The chemical structure of Chloroquine consists of a quinoline ring system with a chlorine atom at the 7-position. At the 4-position of the quinoline, there is a secondary amine group (-NH-) attached to a side chain. This side chain starts with a chiral center (C2) bonded to a methyl group (dashed bond) and a propyl chain. The propyl chain ends at a tertiary amine group bonded to two ethyl groups.</p>
2	Hydroxy-chloroquine	 <p>The chemical structure of Hydroxy-chloroquine is identical to Chloroquine, except that the tertiary amine group at the end of the side chain is substituted with a 2-hydroxyethyl group (-CH<sub>2</sub>-CH<sub>2</sub>-OH).</p>
3	Remdesivir	 <p>The chemical structure of Remdesivir is a complex nucleoside analog. It features a central phosphorus atom (P) bonded to a phenyl ring, a nitrogen atom (NH), and two oxygen atoms. The nitrogen atom is part of a side chain that includes a methyl group and a butyl ester group. The phosphorus atom is also bonded to a ribose sugar ring. The ribose sugar has hydroxyl groups at the 2' and 3' positions and is attached to a guanine base at the 1' position. The guanine base has a cyano group (-C≡N) at the 6-position.</p>

4	Arbidol	 <p>The chemical structure of Arbidol is a complex heterocyclic molecule. It features a central benzimidazole ring system. The benzimidazole ring is substituted with a methyl group on the nitrogen atom, a hydroxyl group (HO), and a bromine atom (Br) on the benzene ring. A side chain consisting of a methylene group and a sulfur atom (S) is attached to the benzimidazole ring, with a phenyl ring attached to the sulfur atom. Another side chain, consisting of a methylene group and an ethoxy group (O-CH2-CH3), is attached to the benzimidazole ring.</p>
5	Oseltamivir	 <p>The chemical structure of Oseltamivir is a cyclohexane ring substituted with several groups. It features a methylamino group (NH-CH3) and a primary amino group (H2N) on the cyclohexane ring. A side chain consisting of a methylene group and a carbonyl group (C=O) is attached to the cyclohexane ring, with an ethoxy group (O-CH2-CH3) attached to the carbonyl group. Another side chain, consisting of a methylene group and an oxygen atom (O), is attached to the cyclohexane ring, with a propyl group attached to the oxygen atom.</p>
6	Galidesivir	 <p>The chemical structure of Galidesivir is a complex heterocyclic molecule. It features a central benzimidazole ring system. The benzimidazole ring is substituted with a cyclopentane ring on the benzimidazole ring. The benzimidazole ring is also substituted with a methyl group on the nitrogen atom, a hydroxyl group (HO), and a bromine atom (Br) on the benzene ring. A side chain consisting of a methylene group and a sulfur atom (S) is attached to the benzimidazole ring, with a phenyl ring attached to the sulfur atom. Another side chain, consisting of a methylene group and an ethoxy group (O-CH2-CH3), is attached to the benzimidazole ring.</p>

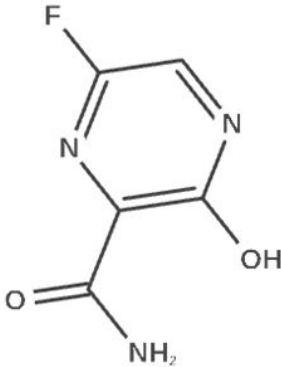
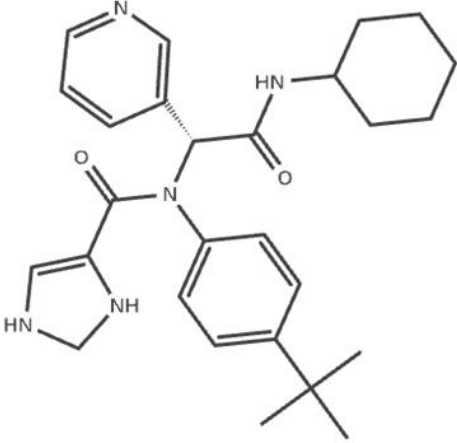
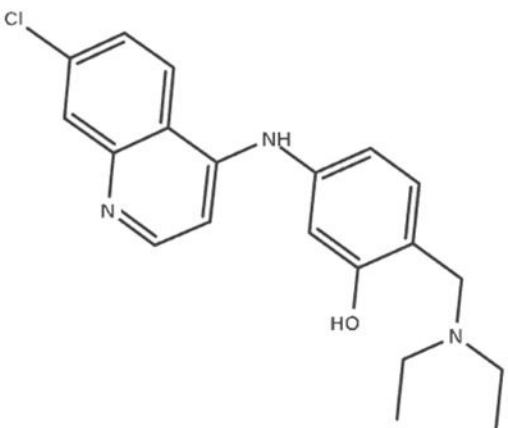
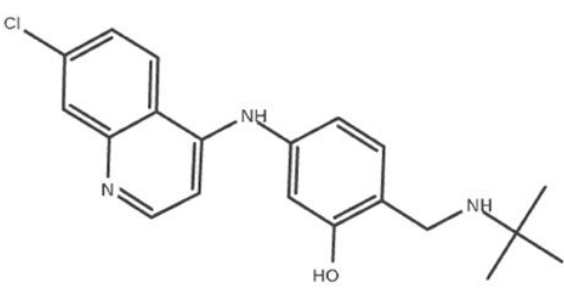
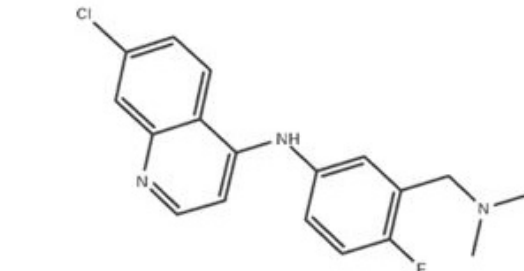
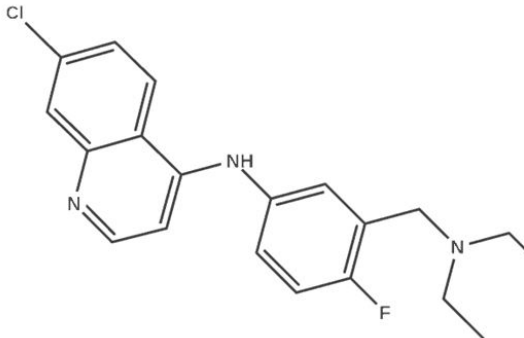
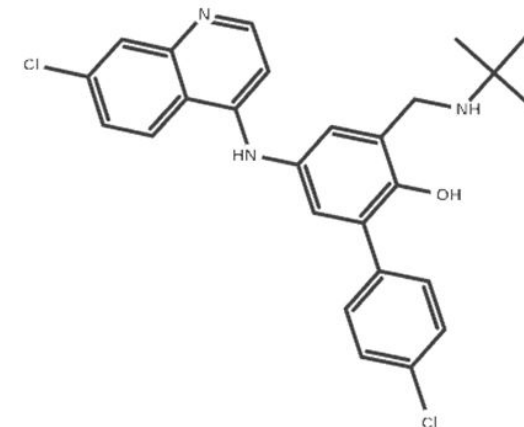
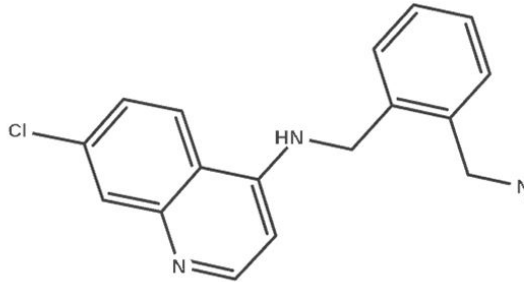
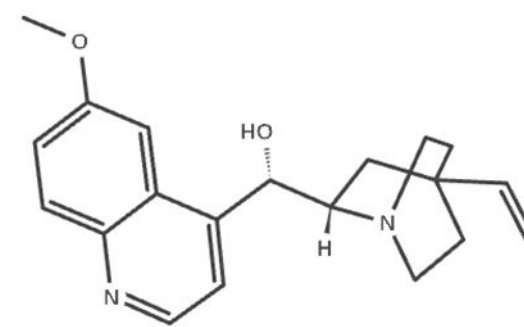
7	Favipiravir	
8	X-77 ligand (inhibitor COVID-19 main protease (Mpro) the 3CL-protease (PDB code: 6W63))	

Table 1: (Structure of compounds)

Chart 1

1	Isoquine	
2	GSK-369796	

3	FAQ- (N-Me <sub>2</sub> )	
4	FAQ- (N-Et <sub>2</sub> )	
5	Tebuquine	
6	Phenylequine	
7	Quinine	

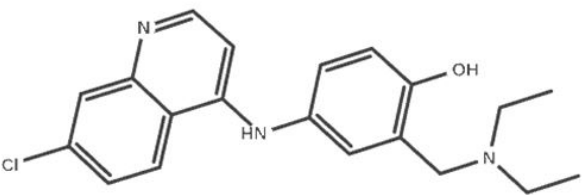
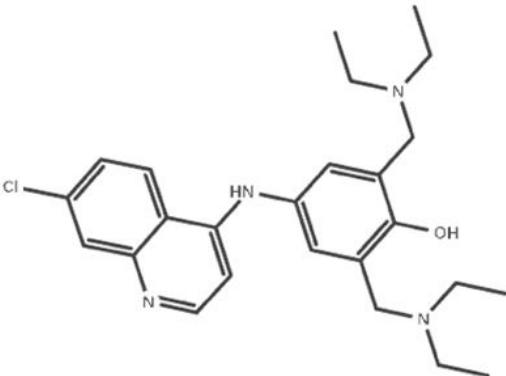
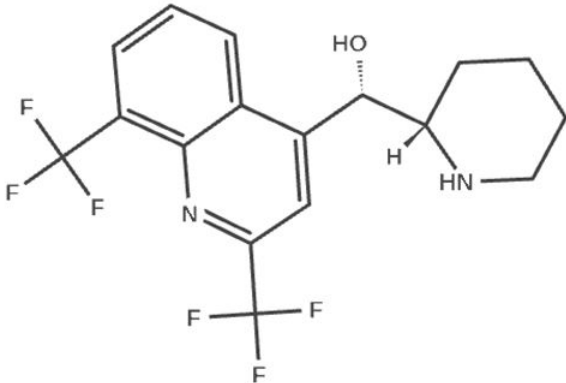
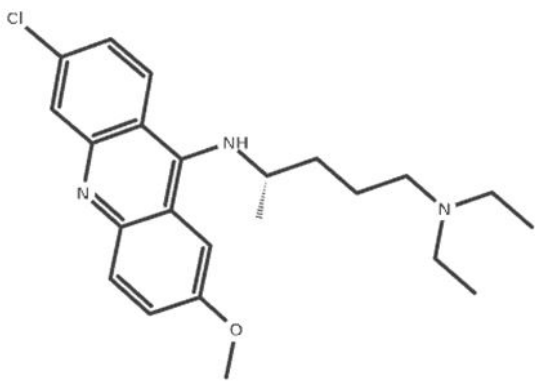
8	Amodiaquine	
9	Cycloquine	
10	Mefloquine	
11	Mepacrine	

Table 1: (Structure of compounds)

Chart 2

Compd (Mol. Wt.)	Dipole moment (debye)	Dipole moment (debye)	Max MEP (+)	PSA (A <sup>2</sup> )	Log P	HBA Count	HBD Count	No Rot. Bonds
1. (319.8)	5.87 (<-quinoline N)	206.1 (on quinoline N)	232.1 (on H of NH group)	17.9	0.66	3	1	8
2. (335.8)	4.43 (<-quinoline N)	197.6 (on quinoline N)	230.9 (on H of NH group)	38.7	-0.20	4	2	9
3. (604.6)	5.27 (<-5-membered ring)	310.2 (N on the 6-mem ring)	205.3 (N of 5 mem NH)	157.9	N/A	12	3	15
4. (477.4)	3.12 (perpend.)	198.3 (Br & OH & -O-)	119.1 (scattered)	35.8	-0.61	5	1	7
5. (312.4)	3.77 (perpend.)	198.0 (O of NH-C (Me)=O)	242.9 (H of NH-C (Me)=O)	73.4	0.19	5	1	9
6. (184.3)	0.56 (<- arom ring)	128.0 (hydrophb aromatic regions)	60.4 (5-membered ring area)	0.0	2.76	0	0	1
7. (157.1)	5.68 (central regions of arom ring and O containg groups)	259.1 (O atom of C=O)	301.1 (H of OH group)	68.0	-1.2	5	2	2
8. (461.6)	4.32 (<- six mem N containing ring)	337.3 (O of C=O, region around N ring)	197.0 (H of NH in the 5-mem ring)	59.9	1.09	6	2	7

Table 2: Stereoelectronic property computations

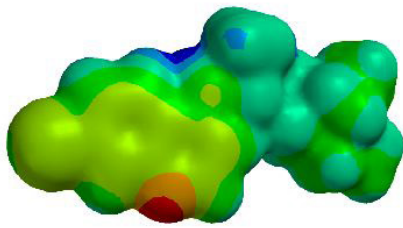
Compd (Mol. Wt.)	Dipole moment (debye)	Min MEP (-) (kJ/mol)	Max MEP (+)	PSA (A <sup>2</sup> )	Log P	HBA Count	HBD Count	No Rot. Bonds
1'. (355.8)	6.5 (<-quinoline N)	195.7 (on quino-line N)	249.6 (on H of OH group)	36.3	-1.19	4	2	7
2'. (355.8)	4.03 (<-quino-line N)	189.8 (on quino-line N)	316.6 (on H of OH group)	44.7	-1.37	4	2	5
3'. (329.8)	5.92 (<-quino-line N)	332.0 (on quino-line N)	195.4 (on H of NH group)	19.0	-1.32	3	1	4
4'. (357.8)	5.08 (<-quino-line N)	331.6 (on quino-line N)	204.5 (on H of NH group)	16.7	-0.64	3	1	6
5'. (466.4)	6.64 (elsewhere)	338.4 (on quino-line N)	198.4 (on H of NH group)	40.2	-0.94	4	2	5
6'. (325.8)	7.57 (<-quino-line N)	351.1 (on quino-line N)	179.0 (on H of NH group)	19.3	-0.33	3	1	5

Compd (Mol. Wt.)	Dipole moment (debye)	Min MEP (-) (kJ/mol)	Max MEP (+)	PSA (Å <sup>2</sup> )	Log P	HBA Count	HBD Count	No Rot. Bonds
7'. (324.4)	2.57 (elsewhere)	331.3 (on the bridge N)	140.5 (on H of OH group)	36.6	-0.29	4	1	5
8'. (355.8)	6.04 (<-quino-line N)	345.4 (terminal -N-butyl)	228.2 (on H of OH group)	36.2	-1.19	4	2	7
9'. (441.0)	8.7 (elsewhere)	359.5 (terminal -N-butyl)	194.0 (on H of NH group)	32.8	-0.89	5	2	11
10'. (378.3)	9.4 (<-quino-line N and CF <sub>3</sub> )	297.91 (on quino-line N)	161.8 (H of OH)	36.7	2.39	3	1	3
11'. (399.0)	4.63 (elsewhere)	175.1 (on anthracene ring N)	161.5 (H of NH)	26.1	1.04	4	1	9

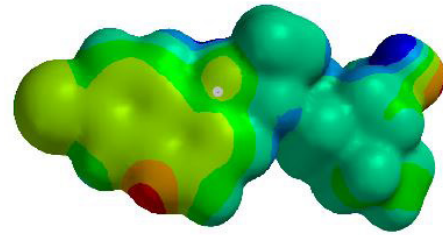
**Table 3:** Stereoelectronic property computations

However, for obtaining a deeper insight on the intrinsic reactive nature of compounds, a computational model based on stereo-electronic properties of all compounds Table 1 (Chart 1 & 2) was developed focusing particularly on the molecular electrostatic potential (MEP) profiles of compounds. MEP profiles are very useful for understanding the intrinsic reactive nature of compounds, particularly in this case for anti-COVID19 activity. The MEP profile of a molecule is created by its own nuclei and electrons with the surrounding space which can be calculated by bringing a bare proton (H<sup>+</sup>) to the proximity of a molecule. The MEP profiles are well-documented as key recognizable features to promote interaction between a molecule and its target structure at longer distances [21]. These profiles are essentially known as “interaction pharmacophore” profiles. The regions of negative potential indicate nucleophilic sites (H-bond acceptor), suitable for electrophilic attractions; conversely the regions of positive potentials indicate electrophilic sites (H-bond donor) and therefore suitable for nucleophilic interaction. Thus, these profiles can provide invaluable information about intrinsic reactivity of molecules. MEP is a real physical property of a molecule related to how a molecule is first “seen” or “felt” by another approaching molecular entity. This property can be determined experimentally through crystallographic diffraction patterns and can also be calculated accurately using quantum chemical computations [21-23]. The calculated MEP profiles can lead a better understanding of complex biological processes involving the charge-dipole, dipole-dipole, and quadrupole-dipole interactions. Since MEP can simultaneously display the molecular shape, size, and charge distributions, the reactive sites of a molecule can be better visualized. These profiles allow us to visualize the variable charged regions of a molecule in terms of color grading. Areas of minimum potential (usually designated as deepest red regions, negative MEP) are characterized by an abundance of electrons or highest electron density or the most nucleophilic site in the molecule. Areas of maximum positive potential, (usually designated as deepest blue, positive MEP), are characterized by a relative absence of electrons or the most electrophilic site in the molecule. Figures (1a & 2a) show MEP on the van der Waals surface of the Table 1 (Chart 1 & 2) compounds respectively.

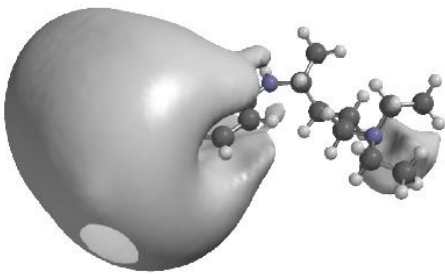
The MEP profiles beyond the van der Waals surface are crucial for determining the recognition capability of the target structure from a distance. The target structure recognizes these features from a distance and accordingly promotes complementary interactions. These profiles for Table 1 (Chart 1 & 2) compounds at approximately -20.0 kJ/mol are shown in Figure (1b & 2b), respectively.



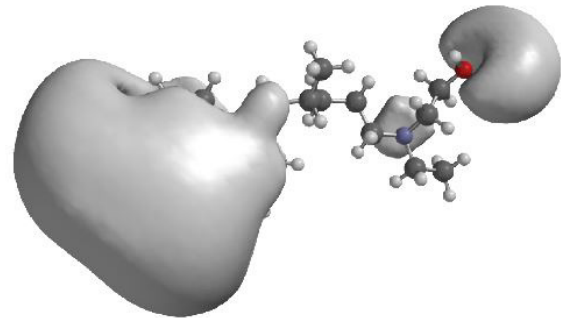
CQ-MEP



HCQ-MEP



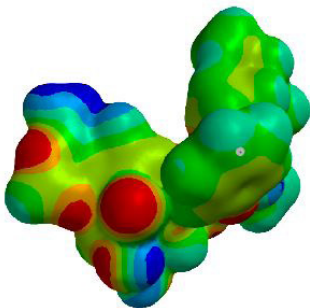
CQ- MEP at -20.0 kJ/mol



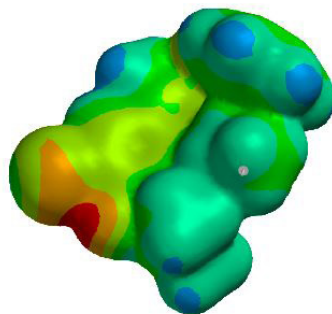
HCQ –MEP at -20.0 kJ/mol

(a) Upper rows: MEPs on the van der Waals surface of the compounds

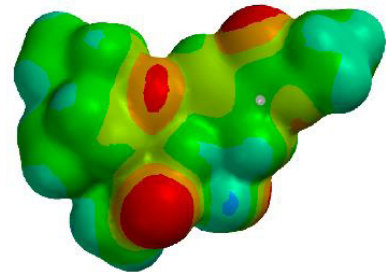
**Figure 1:** Molecular electrostatic potential profiles (MEPs) of Chart 1 compounds



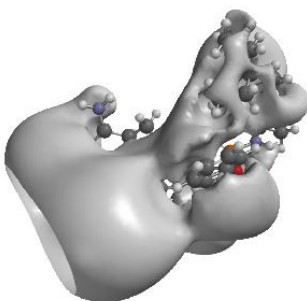
Remdesivir-MEP



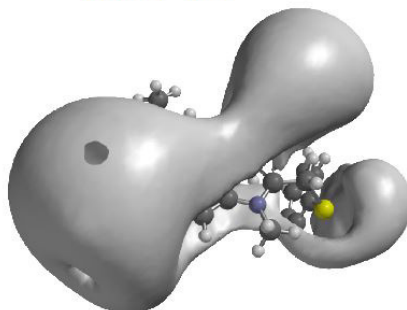
Arbidol -MEP



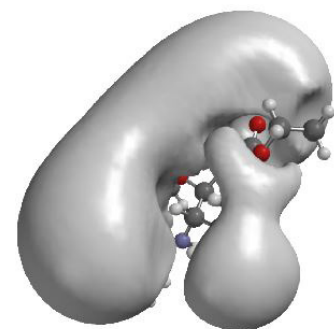
Oseltamivir-MEP



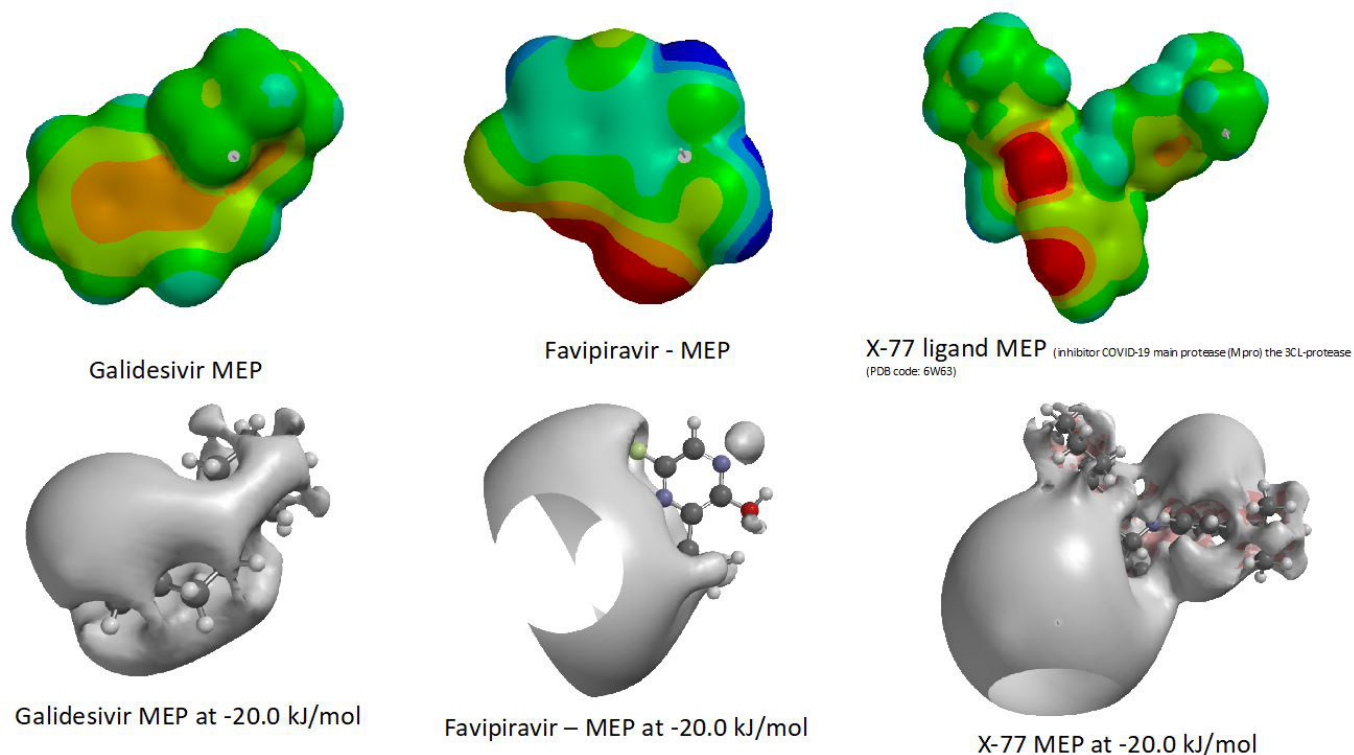
Remdesivir-MEP at -20.0 kJ/mol



Arbidol –MEP at -20.0 kJ/mol



Oseltamivir-MEP at -20.0 kJ/mol



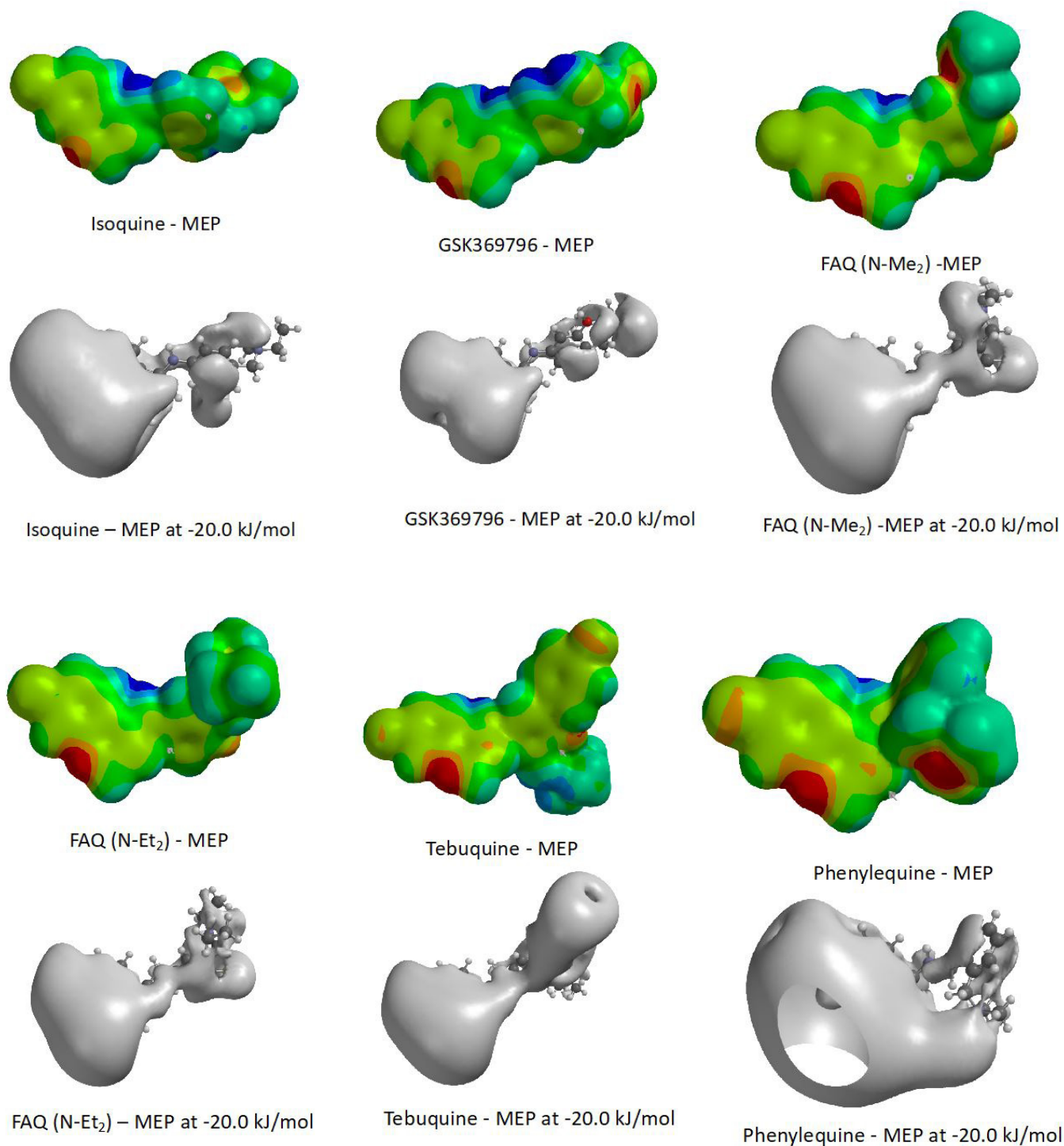
(b) Lower rows: MEPs beyond van der Waals surface (-20.0 kJ/mol) of the compounds

**Figure 1:** Molecular electrostatic potential profiles (MEPs) of Chart 1 compounds

Inspection of Figure 1a indicates that the most prominent negative potential region is by the N atom of the quinoline ring in Compounds 1 (CQ) and 2 (HCQ) (Table 1, Chart 1) whereas Compounds 3-8 (Table 1, Chart 1) show multiple sites of negative potential regions. Thus, it indicates that both Compound 1 & 2 (Table 1, Chart 1) can have one strong hydrogen bond acceptor (HBA) interaction through quinoline N with the active site of the receptor. The other HBA sites in Compound 1 (two HBA sites) & Compound 2 (three HBA sites) are most likely less accessible for hydrogen bond interactions due to steric factors associated with their neighboring atoms. Calculated dipole moment directions toward the quinoline ring N atom in both Compound 1 & 2 (Table 1, Chart 1) are consistent with the MEP profiles. However, for Compounds 3-8 (Table 1, Chart 1), dipole moments point to different directions and so also multiple MEP locations on different electron rich atoms suggesting the possibility of multiple hydrogen bonding interactions with the target molecule. This is also consistent with the number of HBA and HBD counts (Table 2). In addition, large distributions of weak electrostatic potential regions in the molecules (represented by intermediate shades of varying green color, Figure 1) indicate strong hydrophobic interaction capabilities. Interestingly, all compounds of Table 1 (Chart 1) show a large extended electrostatic potential region in one region of the molecule (Figure 1b) indicating one particular region of the molecule to be have maximum recognition effects towards the target receptor. Thus, anti-COVID-19 activity of Table 1 (Chart 1) compounds appears to have both an important role for strong hydrogen bonding as well as hydrophobic interactions with the complementary sites of the target protein. Quinoline ring N atom appears to play a very important role for anti-COVID19 activity in 1 & 2, consistent with the MEP profiles showing the capability of both strong H-bond acceptor and hydrophobic interactions with the complementary site of the target receptor. Apart from the capacity of hydrogen bonding and hydrophobic interactions, the compounds also appear to have the capability for pi-pi stacking or cation-pi interactions in the active site due to the presence of aromatic rings in them. Interactions of pi-pi stacking and/or cation-pi have been reported in the inhibitor bound x-ray crystallographic structure of COVID-19 main protease (M<sup>Pro</sup>) [12,13].

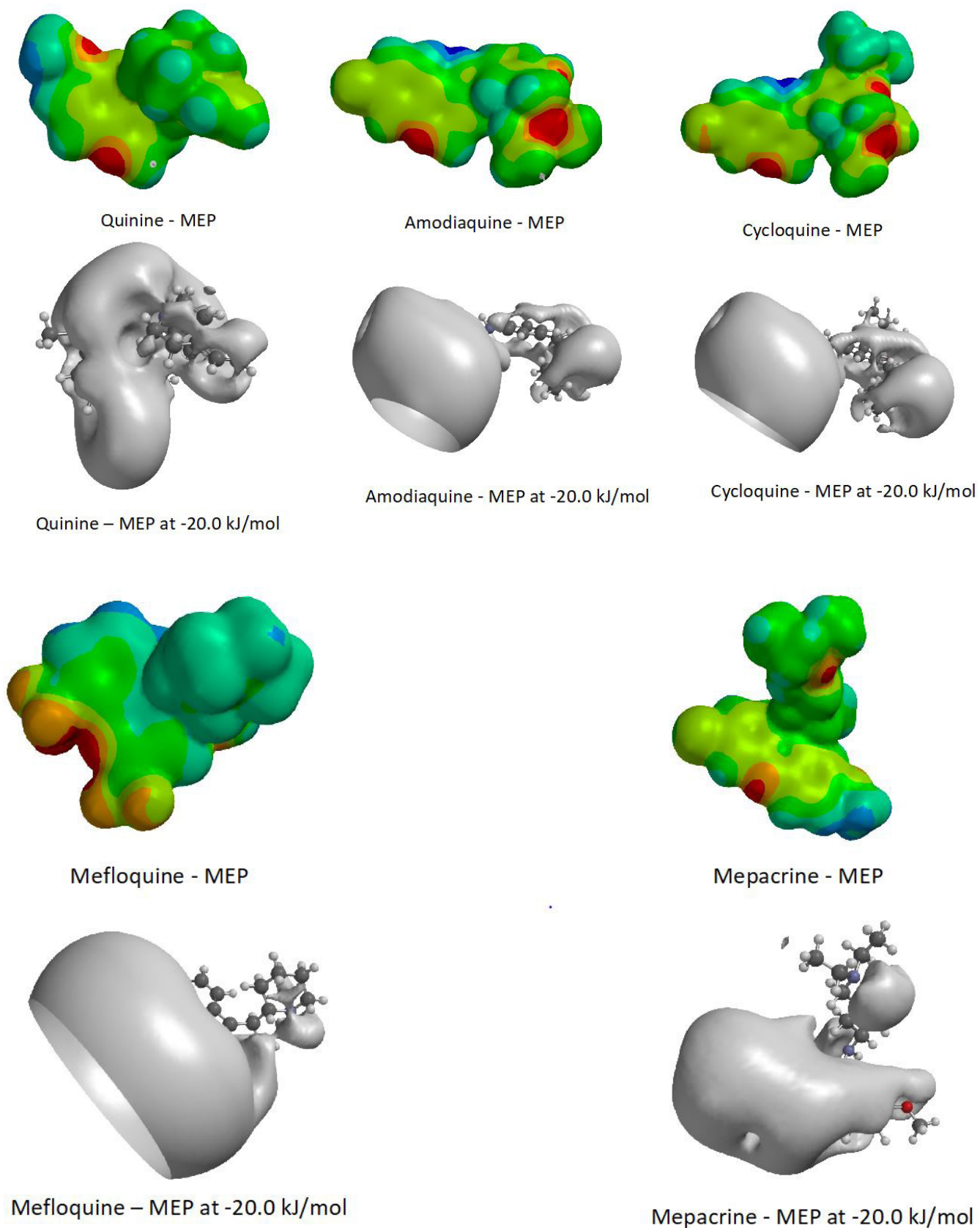
Next, based on the reported anti-COVID-19 activities [1] of 1 (CQ) and 2 (HCQ) Table 1 (Chart 1) and observed MEP profiles, a literature search for 4-aminoquinoline antimalarial compounds [14,15,24] was performed which led to identify eleven 4- aminoquinoline derivatives having the potential of anti-COVID19 activity. The identified compounds are shown in Table 1 (Chart 2). Most of the identified compounds have antimalarial activities and a majority of them was reported to have shown antiviral activities, such as anti-dengue and anti-Zika activities [15, 24]. The stereo-electronic properties and drug-likeness properties of

Table 1 (Chart 2) compounds are shown in Table 2 and discussed earlier. MEP profiles of these compounds are shown in (Figures 2a & 2b). The most negative potential region of the compounds is found to be located by the quinoline nitrogen atoms of all compounds as shown by the deepest red color (Figure 2a). However, in addition to the H-bond acceptor capacity of quinoline nitrogen atom, a few other atoms in the 4- aminoquinoline derivatives too are found to have large negative electrostatic potential regions (red color, Figure 2a) indicating multiple H-bond acceptors capacities of the compounds. However, despite having the capacity of multiple hydrogen bonding interactions, all sites may not have equal accessibilities for the target due to steric factors associated with different regions in the molecules.



(a) Upper rows: MEPs on the van der Waals surface of the compounds

**Figure 2:** Molecular electrostatic potential profiles (MEPs) of Chart 2 compounds



(b) Lower rows: MEPs beyond van der Waals surface (-20.0 kJ/mol) of the compounds.

**Figure 2:** Molecular electrostatic potential profiles (MEPs) of Chart 2 compounds

The MEP profiles of compounds beyond van der Waals surface (Figure 2b) show a large extended potential regions by the quinoline nitrogen atoms. This characteristic recognition feature of suction-like appearance of the electrostatic potential region (Figure 2b) clearly indicates the power of H-bonding potential of the quinoline nitrogen atoms with the complementary active site of the target receptor protein. This characteristic MEP profile of Table 1 (Chart 2) compounds are consistent with the Table 1 (Chart 1) potent COVID-19 active compounds, 1 & 2 and thus, the feature could be potentially linked to anti-COVID-19 activity. Apart from hydrogen bonding capabilities, like the Chart 1 (Table 1) compounds Chart 2 compounds also show large area of weak electrostatic potential and aromatic ring regions (Figure 2a & 2b) indicating the capacity for hydrophobic, pi-pi stacking and cation-pi interactions with the target. Thus, in addition to the important role of strong hydrogen bonding interactions, hydrophobic and weak interactions of the compounds also appear to play significant role for potential anti-COVID19 activity of the identified Table1(Chart 2) compounds.

Since quinoline ring N atom of aminoquinolines in compounds 1 & 2 Table 1 (Chart 1) is reported [1] to play a crucial role for anti-COVID-19 activity by modulating the pH of the medium, the aminoquinolines identified (Table 1, Chart 2) should also have similar potential for anti-COVID-19 activity by modulating the pH of the medium. The mechanism for potent anti-COVID-19 activity of CQ and HCQ treatment is believed to be through a cellular entry process by increasing the pH of endosomes, thereby providing a negative influence on the fusion process of virus and endosome [1]. Thus, consistency of the observed MEP profiles (Figure 2a & Figure 2b) for the identified compounds (Table 1, Chart 2) with CQ & HCQ (Chart 1) indicates the possibility of similar mechanism for anti-COVID-19 activity.

### Pharmacophore analysis from Chemical Function Descriptors (CFD's)

The interaction-pharmacophore model was further analyzed in the light of Chemical Function Descriptors (CFD's) of Table 1 (Chart 1 & 2) compounds by performing scoring function calculations to find out similarity between them. CFDs are descriptors assigned to a molecule based on its chemical behavior to characterize the common features associated amongst different structures. In a chemist's language, the lone pair in a molecule suggests the role of a hydrogen-bond acceptor (HBA) property, and sterically crowded part of the molecule would be hydrophobic because getting close to it would be difficult.

Although the calculated MEP profiles provide more accurate information of intrinsic reactive nature of molecules, the CFDs can provide qualitative assessment by providing useful interaction capacities of molecule. For example, when there are no heteroatoms possibility for hydrogen bonding may be ruled out. Other examples are  $\pi$  system of benzene and aromatics provide. Similar conditions that make the aromatic ring susceptible for electrophilic substitution would also repel other electron-rich regions and would attract electron-poor regions. Perhaps, a medicinal chemist would reach similar conclusions simply by looking at the molecule but the MEP calculations would provide a better accurate assessment of both locations and strength of H-bond acceptor or donor sites. Nonetheless, calculated CFDs of all the compounds and similarity analysis between the known anti-COVID19 and our identified compounds provide a rapid qualitative assessment for potential activity of the compounds.

The similarity analysis provides insight between atom centers in different molecules regarding their likely functions as a hydrogen-bond donor or hydrogen-bond acceptor. Additionally the analysis also provides an estimate of whether an atom center is likely to act on a positive or a negative charge or is hydrophobic. Based on the procedures in Spartan'18, CFD models were generated and defined. Details of the procedure, CPU time and analysis are discussed in the "Material and methods" section. Similarity calculations were performed by creating a library of CFD-based pharmacophore on compounds taken from both Table 1 (Chart 1& 2) and results are presented in Table 4. CFD pharmacophore of the 4-aminoquinolines was based on the possible HBA, HBD and hydrophobic sites which were found to be consistent with their corresponding MEP profiles. The results of the similarity analysis and score of the aminoquinolines with respect to isoquine Table 1 (Compound 1, Chart 2) in terms scores are presented in Table 4a.

Compound	Scores
Table 4a	
1. Isoquine (1, Chart 2)	1.0
2. Chloroquine (1, Chart 1)	0.97
3. HydroxyCQ (2, Chart 1)	0.92
4. GSK369796 (2, Chart 2)	0.92
5. Cycloquine (9, Chart 2)	0.83
6. FAQ-NEt2 (4, Chart 2)	0.77
7. FAQ-NMe2 (3, Chart 2)	0.75
Table 4b	
1. X-77 ligand (8, Chart 1)	1.0
2. HydroxyCQ (2, Chart 1)	0.79
3. Chloroquine (1, Chart 1)	0.52

**Table 4:** Pharmacophore analysis from Chemical Function Descriptors (CFD's)

In order to assess the potential of aminoquinolines to bind to the active site Mpro, another similarity analysis on CFD pharmacophores was carried out between the two known anti-COVID19 compounds CQ, HCQ and the ligand X-77, experimentally reported to be bound in the active site of MPro [12, 25, 26]. The results of this analysis is presented in Table 4b. A cursory glance of Table 4a indicates that isoquine and GSK369796 (compound 1 & 2, Table1, Chart 2) are about ninety percent similar to (compound 1 & 2, Table 1, Chart 1) chloroquine (CQ) and hydroxychloroquine (HCQ). Therefore, isoquine and GSK369796 have high probability for potential activity against COVID-19. This probability is further supported from the scores of Table 4b where HCQ is found to be almost eighty percent similar to the X-77 ligand reported in the bound Mpro protein x-ray crystallographic structure [12, 13, 26-29].

### Structure-based approach for validation of the pharmacophore

Amongst drug targets for coronaviruses, the main protease (Mpro, also called 3CLpro) is believed to be most attractive because it plays an essential role in processing the polyproteins that are translated from the viral RNA. The x-ray crystallographic structures of SARS-CoV-2 Mpro with and without ligand have been reported earlier [26]. In this study, the 3-chymotrypsin-like protease (3CL-protease) structure was analyzed as a target because this enzyme is the main protease used to cleave polyproteins into replication-related proteins [29]. The 3CL-protease structure (PDB code: 6W63) was originally obtained from a taxonomically-driven approach for development of broad-spectrum inhibitors including SARS-CoV-2 (COVID-19). However, it was deposited in the RCSB Protein Data Bank recently [12, 13]. Information obtained from the crystallographic structure of this protein with a bound ligand was used as the structure-based pharmacophore model to assess our calculated “interaction-pharmacophore “model [26].

Analysis of the co-crystallized inhibitor X77 at the binding site of the 3CL-protease structure indicates five hydrogen-bonding interactions connecting its amidic NH with carbonyl of Asn142 via bridging water molecule, the amidic carbonyl with NH of Glu166, the other carbonyl with NH of Gly143, imidazole N with Thr26 via two bridging water molecules, and the fifth hydrogen bond connects the second imidazole N with NH of His41. In addition, two  $\pi$ - $\pi$  stacking interactions are observed. First, between the benzene ring of the potent inhibitor X77 and the imidazole ring of His41, where the second  $\pi$ - $\pi$  stacking involves inhibitor's pyridine ring sandwiched between the benzene ring of Phe140 and the imidazole ring of His172. In addition, the tert-butyl group of X77 is seen to be directed towards Met165 and Cys44 suggesting the existence of mutual hydrophobic interactions, anchoring this inhibitor within the binding pocket of COVID-19 main protease (M<sup>pro</sup>) (Figure 3).

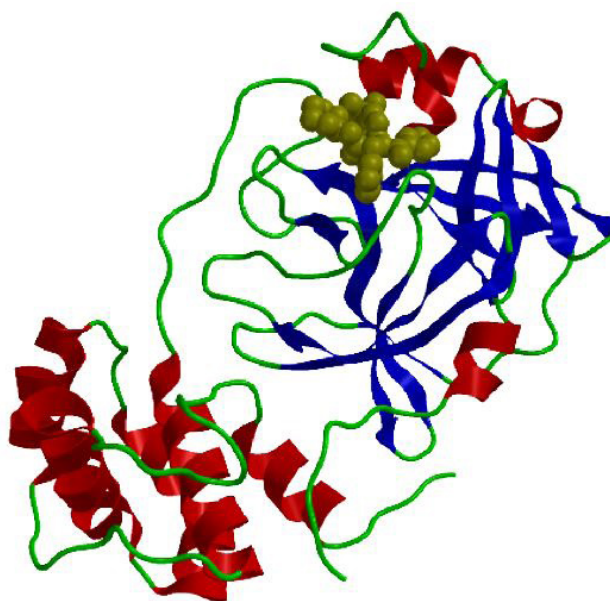


**Figure 3:** 3CL main protease structure (pdb: 6W63) with the ligand X77

The above described interactions for the anti-COVID-19 active inhibitor X77 provide valuable insights to compare our generated pharmacophore model on the identified aminoquinolines. From the above analysis, it is apparent that any pharmacophore model for potential anti-COVID-19 activity should contain features for strong hydrogen bonding interactions having the capacity for at least one hydrogen bond donor (HBD) and multiple H-bond acceptors (HBA) for the ligand. In addition, ring aromaticity (RingArom) and hydrophobic (Hb) features are also necessary [29, 30]. Based on above observations, our calculated interaction pharmacophore model in conjunction with the CFD features appear to be quite consistent. All the isoquine (N-tert-butyl) and 4-aminoquinoline derivatives identified in our study are found to contain 4 or 3 acceptors (HBA), one donor (HBD), two aromatic rings (RingArom) and one hydrophobic feature (Hbic) (Table 2). Thus similar to the tert-butyl group of the ligand (X77) reported above, along with the ability of H-bond interactions in the active site, the aminoquinoline compounds also should have the ability for hydrophobic interactions with Met165 and Cys44 within the binding pocket of COVID-19 main protease (Mpro). Therefore, the 4-aminoquinolines identified by our “interaction pharmacophore model” should have the potential for activity against COVID-19 and the model should have the selectivity for capturing true positive hits in the database searches. Structure-based pharmacophore models obtained from ligand-target structures have shown to be successful alternatives to traditional approaches, particularly evident from their role in the virtual screening [28].

Furthermore, experimental evidence has shown that the EC<sub>90</sub> of CQ against COVID-19 in Vero E6 cells to be 6.90 mM, and suggested to be potentially applicable to COVID-19 patients [1]. In addition, both CQ and HCQ are known to increase the intracellular pH and inhibit lysosomal activity in antigen-presenting cells (APCs), including plasmacytoid dendritic cells (pDCs) and B cells [30]. Since our identified isoquine-aminoquinoline compounds are similar to CQ and HCQ chemical structures Table 1 (compound 1 & 2, Chart 1) and stereoelectronic properties including MEP profiles, the compounds should have the potential for activity against COVID-19. Advantage would be that our identified isoquine derivatives are devoid of toxic properties associated with CQ and HCQ [14, 15].

It is important to note that 4-aminoquinoline antimalarials like amodiaquine can cause adverse side effects including agranulocytosis and liver damage [14 (a), 14 (b)]. The adverse effects of amodiaquine is believed to be due the formation of an electrophilic metabolite, amodiaquine quinoneimine (AQQI), capable for binding with cellular macromolecules to cause hypersensitivity in patients. But isoquine analogs like GSK369796 are not capable of forming the toxic quinoneimine metabolites via cytochrome due to structural modifications accomplished through substitutions of hydroxyl group and Mannich side chain. This would not only prevent oxidation to toxic metabolites but would also retain the bonding interactions with the aromatic hydroxyl function.

Thus, isoquine compounds should have advantage over the known toxicity of the other 4-aminoquinoline derivatives including CQ & HCQ. Furthermore, the isoquine analogue, N-tert-butyl analogue (GSK369796) showed superior pharmacokinetic and pharmacodynamic profiles than isoquine in pre-clinical evaluation studies performed by Glaxo SmithKline pharmaceuticals. The compound was also reported to have moderate to excellent oral bioavailability, low toxicity in in vitro studies, and acceptable safety profile [14,15].

## Concluding Remarks

In this study, a rational approach for discovery of anti-COVID19 compounds is presented. Using simple molecular modeling techniques and analysis of molecular electrostatic potentials, it is possible to identify new class of compounds having the potential for anti-COVID19 activity. Although the identified compounds based on the “interaction pharmacophore” model are yet to be tested experimentally, the compounds are found to be quite similar to CQ and HCQ already used for treatments against COVID-19. Results from our variety of theoretical analysis and the observed consistency with the inhibitor bound x-ray crystallographic structure of the main COVID-19 protein further strengthen this probability. Advantage of the isoquine analogues over CQ & HCQ, particularly GSK369796 should play an important role because this compound is known to be less toxic than other aminoquinolines. It may be worthwhile to mention that GSK369796, N-tert-Butyl isoquine, was rationally designed based on chemical, toxicological, pharmacokinetic and pharmacodynamics properties and developed as part of a public private partnerships involving academics at University at Liverpool, UK, Medicine for Malaria Venture (MMV), and GSK Pharmaceuticals. The drug was investigated in human volunteers (Clinical Trials.gov identifier: NCT00675064). However, the compound showed evidence of electrocardiogram changes and lower-than-expected plasma exposure. GSK discontinued further study on it after the Phase I trial.

However, isoquine and its derivatives are usually less toxic and show much promise for further investigations. In summary, the “interaction pharmacophore” model developed in this study could be the foundation and useful for further discovery of less toxic anti-COVID-19 compounds.

## Conflicts of Interests

The author declares no conflict of interest.

## Acknowledgements

Georgetown University Medical Center -COVID-19 research for computational facilities.

## References

1. Zhou D, Dai SM, Tong Q (2020) COVID-19: A recommendation to examine the effect of hydroxychloroquine in prevent in infection and progression, *J Antimicrob Chemother* 75: 1667-70.
2. WHO bulletin (2021) 25 April; update.
3. Kruse RL (2020) Therapeutic strategies in an outbreak scenario to treat the novel coronavirus originating in Wuhan, China.
4. Nishimura Y, Hara H (2018) Editorial: Drug Repositioning: Current Advances and Future Perspectives. *Front Pharmacol* 9: 1068.
5. Pushpakom S, Iorio F, Eyers PA, Escott KJ, Hopper S, et al. (2019) Drug repurposing: progress, challenges and recommendations. *Nat Rev Drug Discov* 18: 41-58.
6. Pizzorno A, Padey B, Terrier O, Rosa-Calatrava M (2019) Drug Repurposing Approaches for the Treatment of Influenza Viral Infection: Reviving Old Drugs to Fight Against a Long-Lived Enemy. *Front Immunol* 10: 531.
7. Zheng W, Sun W, Simeonov A (2018) Drug repurposing screens and synergistic drug-combinations for infectious diseases. *Br J Pharmacol* 175:181- 91.
8. Ianevski A, Andersen PI, Merits A, Bjoras M, Kainov D (2019) Expanding the activity spectrum of antiviral agents. *Drug Discov Today* 24: 1224-28.
9. Li G, De Clerck E. Therapeutic options for the 2019 coronavirus (2019s-Cov) (2020) *Nature Reviews Drug Discovery* 19: 149-50.
10. Liu Q, Xuemin-Fang X, Lu T, Chen X, Chung U, et al. (2020) The effect of Arbidol Hydrochloride on reducing mortality of Covid-19 patients: a retrospective study of real world data from three hospitals in Wuhan.
11. Wu R, Wang L, Kao HD, Shannar A, Peter R, et al. (2020) An Update on Current Therapeutic Drugs Treating COVID-19. *Curr Pharmacol Rep.* 11: 1-15.
12. <http://www.rcsb.org/structure/6W63>.
13. Yang H, Yang M, Ding Y, Liu Y, Lou Z, et al. (2003). The crystal structures of severe acute respiratory syndrome virus main protease and its complex with an inhibitor. *Proceedings of the National Academy of Sciences*, 100: 13190-5.
- 14(a). O'Neill PM, Barton VE, Ward SA, Chadwick J (2012) 4-aminoquinolines: chloroquine, amodiaquine and next-generation analogues. In: Staines, H.M.; Krishna, S. (Eds.), *Treatment and Prevention of Malaria*. Springer Basel AG.
- 14(b). O'Neill PM, Mukhtar A, Stocks PA, Randle LE, Hindley S, et al. 2003) Isoquine and related amodiaquine analogues: a new generation of improved 4-aminoquinoline antimalarials. *J Med Chem* 46:4933-45.
15. Balasubramanian A, Teramoto T, Kulkarni AA, Bhattacharjee AK, Padmanabhan R (2017) Antiviral activities of selected antimalarials against dengue virus type 2 and Zika virus. *Antivir Res* 137: 141-50.
16. Spartan'18 Software from Wavefunction, Inc., (2020).

17. Stewart JJ (2004) Optimization of parameters for semiempirical methods IV: extension of MNDO, AM1, and PM3 to more main group elements. *J Mol Model* 10:155-64.
18. Hehre WJ (2003) *A Guide to Molecular Mechanics and Quantum Chemical Calculations*, Wavefunction, Inc, 18401 Von Karman Ave., Suite 370, Irvine, CA 92612,.
- 19(a). Lipinsky CA (2004) Lead- and drug-like compounds: the rule-of-five revolution. *Drug Discov Today: Technologies*.
- 19(b). Rishton GM Review. *Drug Discov Today* 8: 86-96.
20. Gleeson MP (2008) Generation of a set of simple, interpretable ADMET rules of thumb. *J Med Chem* 28: 51: 817-34.
21. Tomasi J, Mennucci B, Cammi R (2005) Quantum mechanical continuum solvation models. *Chem Rev* 105: 2999-3093.
22. Nusser T, Balogh T, Naray-Szabo G (1993) The average molecular electrostatic field as a QSAR descriptor: 5. Hydrophobicity indices for small molecules. *J. Mol Structure* 297:127-32.
23. Leach AR (1998) *Molecular Modelling, Principles and Applications*, A.W. Longman Ltd., Essex CM20 2JE, England.
24. Boonyasuppayakorn S, Reichert ED, Manzano M, Nagarajan K, Padmanabhan R (2014) Amodiaquine, an antimalarial drug, inhibits dengue virus type 2 replication and infectivity. *Antivir Res* 106: 125-34.
25. Zhang L, Lin D, Sun X, Curth U, Drosten C, et al. (2020) Crystal structure of SARS-CoV-2 main protease provides a basis for design of improved  $\alpha$ -ketoamide inhibitors. *Science* 368: 409-12.
26. Jin Z, Du X, Xu Y, Deng Y, Liu M, et al. (2020) Structure of Mpro from COVID-19 virus and discovery of its inhibitors. bioRxiv. RCSB Protein Data Bank.
27. Arooj M, Sakkiyah S, Kim S, Arulalapperumal V, Lee KW (2013) A combination of receptor-based pharmacophore modeling & QM techniques for identification of human chymase inhibitors. *PLoS One* 8: (4).
28. Gaurav A, Gautam V, Pereira S, Alvarez-Leite J, Vetri F, et al. (2014) Structure-based three-dimensional pharmacophores as an alternative to traditional methodologies. *J Recept Ligand and Channel Res* 7: 27-38.
29. Sanders MP, McGuire R, Roumen L, de Esch IJ, de Vlieg J, et al. (2012) From the protein's perspective: the benefits and challenges of protein structure-based pharmacophore modeling. *Med Chem Comm* 3: 28-38.
30. Vincent MJ, Bergeron E, Benjannet S, Bobbie RE, Pierre ER, et al (2005) Chloroquine is a potent inhibitor of SARS coronavirus infection and spread. *Virology* 2:69.